Decoding Glutamate Receptor Activation by the Ca^{2+} Sensor Protein Hippocalcin in Rat Hippocampal Neurons

Alexandr V. Dovgan[1], Volodymyr P. Cherkas[1], Andrey R. Stepanyuk[1], Daniel J. Fitzgerald[2], Lee P. Haynes[2], Alexei V. Tepikin[2]; Robert D. Burgoyne[2], and Pavel V. Belan[1]

[1]Department of General Physiology of the Nervous System, Bogomoletz Institute of Physiology, Kiev 01024, Ukraine, and [2]Physiological Laboratory, School of Biomedical Sciences, University of Liverpool, Liverpool L69 3BX, England, UK.

Correspondence should be addressed to Pavel V. Belan, Department of General Physiology of the Nervous System, Bogomoletz Institute of Physiology, Kiev 01024, Ukraine. E-mail: pasha@biph.kiev.ua.

Running Title**: Decoding Glutamate Receptor Activation by Hippocalcin**

The total number of pages: ?44; figures: ?7; tables: 0; equations: 0.
The total number of words in the whole manuscript: ?10242; in the Abstract: ?249; in the Introduction: 425.

Keywords: Signal transduction; Translocation; Synapse; NCS proteins; NMDA receptors.

Abstract

Hippocalcin is a Ca^{2+}-binding protein that belongs to a family of neuronal Ca^{2+} sensors and is a key mediator of many cellular functions including synaptic plasticity and learning. However, the molecular mechanisms involved in hippocalcin signalling

remain illusive. Here we studied whether glutamate receptor activation induced by locally applied or synaptically released glutamate can be decoded by hippocalcin translocation. Local AMPA receptor activation resulted in fast hippocalcin-YFP translocation to specific sites within a dendritic tree mainly due to AMPA receptor-dependent depolarization and following Ca^{2+} influx via voltage-operated calcium channels. Short local NMDA receptor activation induced fast hippocalcin-YFP translocation in a dendritic shaft at the application site due to direct Ca^{2+} influx via NMDA receptor channels. Intrinsic network bursting produced hippocalcin-YFP translocation to a set of dendritic spines when they were subjected to several successive synaptic vesicle releases during a given burst whereas no translocation to spines was observed in response to a single synaptic vesicle release and to back-propagating action potentials. The translocation to spines required Ca^{2+} influx via synaptic NMDA receptors in which Mg^{2+} block is relieved by postsynaptic depolarization. This synaptic translocation was restricted to spine heads and even closely (within 1-2 μm) located spines on the same dendritic branch signalled independently. Thus, we have concluded that hippocalcin may differentially decode various spatio-temporal patterns of glutamate receptor activation into site and time specific translocation to its targets. Hippocalcin also possesses an ability to produce local signalling at the single synaptic level providing a molecular mechanism for homosynaptic plasticity.

Introduction

Complex spatio-temporal changes in free cytosolic calcium concentration ($[Ca^{2+}]_i$) are decoded into changed activity of effector molecules by various Ca^{2+} sensor proteins. A new emerging concept of cellular signal transduction suggests a dynamic model in which sensor proteins can translocate and undergo reversible binding interaction with the effector proteins rather than being solely activated by the rapid diffusion of Ca^{2+} (Teruel & Meyer, 2000). Local signalling events have been well studied for Ca^{2+} while studies of molecular and cellular mechanisms underlying the signalling of Ca^{2+} sensor proteins in living neurons have only began to emerge.

The neuronal calcium sensor (NCS) proteins, to which hippocalcin studied in this work belongs, constitute a subfamily of EF-hand calcium binding proteins mainly expressed in neurons and neuroendocrine cells (Burgoyne et al., 2004). Recent works have established their involvement in a wide range of Ca^{2+}-dependent signalling processes including modulation and trafficking of ion channels, neurotransmitter release, synaptic plasticity, control of apoptosis and gene expression (McFerran et al., 1998; Jinno et al., 2004; Korhonen et al., 2005; Palmer et al., 2005; O'Callaghan et al., 2005; Zheng et al., 2005; Jo et al., 2008). Information is also available regarding the involvement of NCS proteins in cancer, schizophrenia and several neurodegenerative disorders including Alzheimer's disease (Braunewell, 2005).

Hippocalcin possesses a Ca^{2+}-myristoyl switch, a Ca^{2+}-dependent conformation transition leading to protrusion of its myristoyl-containing hydrophobic N-terminal region out of a hydrophobic pocket (Ames et al., 1997). This allows hippocalcin to translocate to membranes upon Ca^{2+} binding that can be used in signal transduction processes (Kobayashi et al., 1993; O'Callaghan et al., 2003). Hippocalcin is highly

expressed in the hippocampal neurons, in particular in their dendrites, suggesting that it might be involved in postsynaptic signalling. It has been shown that Ca^{2+}-dependent hippocalcin activation in hippocampal neurons is one of the necessary steps involved in expression of NMDA receptor (NMDAR) dependent long-term depression (LTD) (Palmer et al., 2005) and in production of a slow afterhyperpolarization (sAHP) (Tzingounis et al., 2007). These and other hippocalcin-dependent signalling processes involve activation of postsynaptic glutamate receptors. However, it is still unknown if hippocalcin does translocate in living hippocampal neurons in response to glutamate receptor stimulation. We hypothesized that complex changes in Ca^{2+} concentration induced by glutamate receptor activation could result in hippocalcin signalling via its partitioning between a cytosol and specific sites at the plasma membrane in dendrites and spines of hippocampal neurons. In order to test this hypothesis we examined Yellow Fluorescent Protein-tagged hippocalcin (hippocalcin-YFP) translocation induced in transiently transfected hippocampal cultured neurons by iontophoretically applied and synaptically released glutamate.

Materials and Methods

Tissue cultures. All procedures used in this study were approved by the Animal Care Committee of Bogomoletz Institute of Physiology and conform to the Guidelines of the National Institutes of Health on the Care and Use of Animals. Neurones were obtained from newborn rats (age postnatal day 0–1; 56 animals of both sexes for the whole work) killed via rapid decapitation without anaesthesia. Hippocampi of the rats were enzymatically dissociated with trypsin. The cell suspension at an initial density of 3 - 5 ^{x} 10^5 cells per cm^3 was plated on glass coverslips coated with laminin and poly-L-ornithine (Invitrogen, USA). Cells were maintained in feeding solution consisted of

minimal essential medium, 10% horse serum and N2 supplement (Invitrogen, USA) in humidified atmosphere containing 5% CO_2 at 37°C as earlier described (Melnick et al., 1999).

Plasmids. Hippocalcin-YFP, hippocalcin-CFP and enhanced yellow and cyan fluorescent protein (YFP, CFP) plasmids were prepared as described previously (O'Callaghan et al., 2002).

Transient transfection. Hippocampal neurons were transfected after 13-17 days in culture using Lipofectamine 2000 transfection reagent essentially as described by a supplier (Invitrogen, USA). All cultures were used for the experiments on 2-3 days after transfection. A transfection success rate was from 0.2 to 1.0%.

Electrophysiological recordings. Neurons growing in the cultures were visualized using inverted microscopes (IX70 or IX71, Olympus, Germany). Whole-cell patch-clamp recordings in either current- or voltage-clamp mode were obtained using an EPC-10/2 amplifier controlled by PatchMaster software (HEKA, Germany).

A composition of extracellular solution was as follows (mM): NaCl 150; KCl 2; $CaCl_2$ 2; $MgCl_2$ 1; HEPES 10; glucose 10; glycine 0.01; pH 7.3; osmolarity 320 mOsm. Some experiments were carried out in presence of D-2-amino-5-phosphonopentanoic acid (APV, 40μM) or 6-cyano-7-nitroquinoxaline-2,3-dione (CNQX, 10 μM). If other is not indicated gabazine (1μM) or bicuculline (10μM) were always present in the extracellular solution to block $GABA_A$ receptors. An intracellular solution contained (mM): K-gluconate 118, KCl 30; NaCl 5; $CaCl_2$ 0.3; EGTA 1; MgATP 2; GTP 0.3; HEPES 10; pH 7.3; osmolarity 290 mOsm. In some experiments conducted in a voltage clamp mode K^+ was replaced with Cs^+ and 3-5 mM of QX-314, an intracellular sodium channel blocker, were added. Patch electrodes were pulled to obtain a resistance of 4-6

MΩ. Membrane voltage or transmembrane current were low-pass filtered (3 kHz) and acquired at 10kHz. Recordings with a leak current >200pA or a series resistance of >30MΩ were discarded.

Iontophoretic glutamate application was performed via electrodes using a second channel of EPC-10/2 amplifier. The iontophoretic electrodes were filled with a solution containing sodium glutamate (15-150 mM), HEPES (10mM) and NaCl to give final osmolarity of 310 mOsm; pH 7.3 with NaOH. The electrode resistance was in range 80-120 MΩ when filled with a glutamate containing solution. Current pulses of 100 nA with duration of 0.1-2.0 s were produced in a current clamp mode in order to locally apply glutamate while a breaking current of 1-5 nA was engaged between the pulses to prevent leakage of glutamate.

All experiments were conducted at room temperature.

Hippocalcin-YFP translocation imaging. Time-lapse imaging of hippocampal neurons transiently transfected with fluorescent protein(s) was performed using TILL Photonics wide-field imaging system (TILL Photonics, Germany) controlled by TILLvision software. An acquisition rate of Imago CCD camera was varied to precisely record fast changes in hippocalcin-YFP fluorescence and typically was in a range of 0.5-2 Hz. A customized routine written in TILLvision software was used to calculate relative changes in hippocalcin-YFP fluorescence against initial baseline level in order to determine sites of hippocalcin-YFP fluorescence changes. A value of translocation, $\Delta F/F$, was expressed as relative changes in hippocalcin-YFP fluorescence.

The following routine was used to determine translocation sites, over which regions of interest (ROIs) were placed and averaged values of hippocalcin-YFP fluorescence were calculated to demonstrate spatio-temporal patterns of hippocalcin-YFP translocation.

Base and shifted movies were generated based on an initial movie recorded during imaging experiments. Each frame of base movie was generated by averaging 2 to 5 frames of initial movie; each frame of shifted movie was generated by averaging the same number of frames (2 to 5 frames, respectively) of initial movie with 2-7 frame shift between base and shifted movies. The particular number of frames for averaging and shifting depended on kinetics of hippocalcin-YFP translocation transients and acquisition frame rate. The base movie was subtracted from the shifted movie. The resulting differential movie was spatially filtered by an averaging filter with 3x3 kernels. Translocation sites were determined as simply connected regions with a level of hippocalcin-YFP fluorescence 3-4% higher than the baseline fluorescence.

Total hippocalcin-YFP fluorescence in a field of view was calculated for each frame during prolonged experiments and values of fluorescence in regions of interest were normalized to the total fluorescence to compensate for protein photobleaching. In some experiments strong glutamate applications induced photobleaching-independent temporal decrease of hippocalcin-YFP fluorescence up to 5% of initial value. Most probably this decrease was due to intracellular acidification (Micheva et al., 2001) that resulted in a decrease of YFP fluorescence. When hippocalcin-CFP was used instead of hippocalcin-YFP this decrease in fluorescence was almost negligible confirming the relative independence of CFP fluorescence on pH compared to YFP. Since hippocalcin-YFP was mainly used as the hippocalcin sensor in this study and acidification-dependent decrease of YFP fluorescence is not related to the protein translocation we also normalized ROI values to the total value of hippocalcin-YFP fluorescence in a field of view to compensate for this decrease.

In order to observe hippocalcin-YFP translocation without substantial disturbing of intrinsic $[Ca^{2+}]_i$ regulation we mainly studied the translocation during first 10-15 min after establishing a patch clamp configuration or in distal parts of dendritic tree (100-350 μm from soma).

Statistics. Quantitative results are presented as mean ± S.E.M., and statistical significance between groups was tested using Student's *t*-test, with a confidence level of 0.05. The mean for each experiment was calculated as the average for all neurons tested with a given protocol with the exception of experiments with spines. In the latter case the mean was calculated as the average for all ROIs placed over spines.

Chemicals. Glutamate and $GABA_A$ receptor antagonists were obtained from Tocris (Bristol, UK) or Ascent Scientific (Bristol, UK). All other chemicals were purchased from Sigma (USA) and Invitrogen (USA).

Results

Ionotropic glutamate receptor activation induces hippocalcin-YFP translocation

Cultured rat hippocampal neurons were transfected to express hippocalcin-YFP. During time-lapse imaging, intact (not clamped) neurons expressing hippocalcin-YFP were stimulated locally with short (100-1000 ms, 100 nA) iontophoretic glutamate applications delivered from a glass microelectrode placed near an apical dendrite. The glutamate applications resulted in a fast (rise time of 1-2 s) hippocalcin-YFP translocation to a set of sites (sizes of 0.5-2.5 μm) on the dendritic tree (Fig 1A, B). These sites were often located at dendritic branching points or initial parts of dendritic protrusions. At the same time, no translocation to heads of dendritic spines was

observed. The translocation sites did not remain confined to the stimulation area but instead synchronously covered the whole dendritic tree in the field of view. The initial hippocalcin-YFP distribution was restored within 5-15 s after local stimulation and reproducible translocation to the same set of sites on the dendritic tree could be sequentially observed (Fig 1A, B; n=6 neurons). An increase in hippocalcin-YFP concentration in translocation sites was accompanied by a decrease in neighbouring sites keeping the total value of hippocalcin-YFP fluorescence constant during a time course of translocation (Markova et al., 2008). In neurons co-transfected to express hippocalcin-YFP and CFP or hippocalcin-CFP and YFP no changes in free CFP or YFP concentration in translocation sites were observed during the glutamate applications and respective hippocalcin-FP translocation (data not shown; see (Markova et al., 2008)). The hippocalcin-YFP translocation was completely blocked by a cocktail of ionotropic glutamate receptor antagonists CNQX (10 μM) and APV (40 μM) (16.3±2.5% for control, -0.7±0.3% under the blockers and 18.0±3.3% in washout; 46 ROIs, 6 cells, $p < 0.01$ for blockers vs. control and washout; Fig.1C). Thus, we conclude that the observed changes of hippocalcin-YFP fluorescence are ionotropic glutamate-receptor-dependent translocation of hippocalcin-YFP.

In order to check whether both AMPA receptors (AMPARs) and NMDARs contribute to hippocalcin translocation we separately activated these types of receptors. The next series of experiments was conducted in a constant presence of APV (40 μM) to completely block NMDARs. A local iontophoretic glutamate application to an intact (not clamped) neuron induced fast, synchronous and reversible hippocalcin-YFP translocation to many sites in a soma and dendritic tree of stimulated neuron that occurred within the whole field of view. As in the previous series of experiments,

hippocalcin-YFP translocation to dendritic spines was not observed (Fig.2 A,B,C). The translocation was completely blocked by the AMPAR antagonist CNQX (10 μM) (15±2% in control versus 1.2±0.5% in presence of the antagonist; 65 ROIs, 3 neurons, $p<0.001$, Fig. 2 C). Thus, AMPAR activation alone can induce hippocalcin translocation. The synchronous nature of this translocation in the very remote parts of dendritic tree suggests that action potential (AP)-induced voltage-operated Ca^{2+} channel (VOCC) activation may underlie the translocation. In line with this suggestion, AMPAR-dependent hippocalcin-YFP translocation was mainly abolished when the neuronal membrane potential was clamped at -70 mV (0.7±0.3% Fig. 2D, E; 38 ROIs, 5 neurons). The subsequent glutamate application to the same neurons held in a current clamp mode induced neuronal depolarization and burst of APs riding on the top of depolarization transients and a robust translocation (13±3% n=5, $p<0.001$ compared to -70 mV; Fig.2D, E; 38 ROIs, 5 neurons). Trains of back propagating APs (bpAPs) at 50 Hz with duration comparable to one of glutamate-induced depolarization resulted in hippocalcin-YFP translocation to the same sites. However, pooled results showed that AMPAR-dependent translocation in the current clamp mode is significantly larger than bpAP-induced events (13±3% during AMPAR activation versus 7±1% during bpAP trains; $p<0.01$; Fig. 2D, E; 38 ROIs, 5 neurons). Most probably, this discrepancy was due to difference in patterns of VOCC activation induced by different stimulation protocols. Nevertheless, it is clear that the most part of AMPAR-dependent hippocalcin-YFP translocation is due to indirect action of glutamate resulting in AMPAR-dependent depolarization and following VOCC activation.

As the next step glutamate was iontophoretically applied to neurons in presence of AMPAR antagonist, CNQX (10 μM). Recordings were performed in Mg^{2+} free

extracellular solution in order to relieve NMDARs from Mg^{2+} block. In neurons clamped at -60 mV glutamate application induced an inward current and spatially restricted hippocalcin-YFP translocation to many sites. Both the translocation and current were completely blocked by NMDAR antagonist, APV (40 μM; Fig. 3A-C; 16.6±2.8% in control versus 2.8±1.1% under the antagonist, and 6.9±2.3 in washout and 222±37 pA in control versus 27±7 pA under the antagonist and 195±42 pA in washout for the translocation and current, respectively, $p<0.01$ control versus antagonists for both translocation and currents; 53 ROIs, 5 neurones). Hippocalcin initially translocated to sites proximal to the iontophoretic electrode and afterwards translocation events spread along the dendrite with a rate of 20-30 μm/sec (Fig.3D; 5 neurons; at least 2 applications to each neuron), which is close to the rate of glutamate diffusion in the extracellular solution. Thus, direct activation of synaptic and extrasynaptic NMDARs by a diffusion wave of glutamate and respective Ca^{2+} influx to the dendritic shaft is probably the only reason for observed hippocalcin-YFP translocation to certain sites of dendritic plasma membrane.

As shown above no translocation in response to glutamate application was observed in a cocktail of AMPAR and NMDAR blockers. This suggests that metabotropic glutamate receptor activation alone, that may result in inositol 1,4,5-triphosphate (IP_3)-dependent Ca^{2+} mobilization in hippocampal neurons, did not induce $[Ca^{2+}]_i$ elevations that are high enough to produce hippocalcin signalling via its translocation. Nevertheless, metabotropic receptors might contribute to intracellular Ca^{2+} mobilization when Ca^{2+} influx is induced by ionotropic glutamate receptor activation since IP_3 receptors are both Ca^{2+} and IP_3-dependent (Bezprozvanny, 2005). Therefore, glutamate-induced hippocalcin-YFP translocation was compared in extracellular solutions lacking or

containing metabotropic glutamate receptor antagonists, α-methyl-4-carboxyphenylglycine (MCPG) (300 μM). No significant changes in spatio-temporal patterns and amplitudes of translocation were observed in neuronal dendritic trees under study (12.0±4.4% without MCPG versus 11.4±4.4% during antagonist perfusion; 23 ROIs, 4 neurons, p=0.22; data not shown), indicating that metabotropic glutamate receptor activation does not contribute to hippocalcin signalling at least in the case of local stimulation.

The other mechanism that may take part in hippocalcin translocation during glutamate stimulation is Ca^{2+}-dependent Ca^{2+} release from the endoplasmic reticulum (ER) (Bardo et al., 2006). However, no changes in hippocalcin-YFP translocation in the dendritic tree was observed when cultures were incubated with the ER Ca^{2+}-ATPase blocker, CPA (10 μM) (8.3±2.3% in control versus 7.4±1.2% during CPA perfusion and 8.5±0.9% in washout; 26 ROIs, 4 neurons, p=0.26).

Thus, we have shown above that NMDARs are the only glutamate receptors whose local activation induces site-specific hippocalcin translocation. Taking into account that activity-dependent release of glutamate in glutamatergic synapses should lead to synaptic NMDAR activation we aimed to check if such activation might result in hippocalcin translocation.

Synaptic NMDAR activation induces local spine-specific hippocalcin translocation

Neurons in the hippocampal cultures under study revealed both miniature and activity-dependent excitatory postsynaptic potentials (EPSPs) with one or few APs riding on the top of some EPSPs. Neither of these two types of spontaneous synaptic activity resulted

in measurable hippocalcin-YFP translocation indicating that properties of this neuronal Ca^{2+} sensor are well positioned to filter low-frequency synaptic and AP activity. Reducing [Mg^{2+}] below physiological levels induces enhanced excitability in both hippocampal slices (Walther et al., 1986) and cultures (Mangan & Kapur, 2004). It has been shown that this formulation of extracellular solution is also a means to selectively activate synaptic rather than extrasynaptic NMDARs (Lu et al., 2001). In our hands in a nominally zero external Mg^{2+} medium with a $GABA_A$ receptor blocker, gabazine (1 μM), and AMPAR blocker, CNQX (10 μM), neurons demonstrated recurrent spontaneous action potential bursts superimposed on prolonged depolarization. In a voltage clamp mode (-70 mV) this spontaneous network activity resulted in bursts of inward postsynaptic currents completely blocked by APV (40 μM) (data not shown). It indicates that NMDARs are involved in generation of these postsynaptic currents. Having in mind that NMDARs are relieved of Mg^{2+} block in Mg^{2+} free solution, they are probably the only source of Ca^{2+} that could potentially induce hippocalcin translocation in pyramidal neurons clamped at -70 mV. During imaging of neuronal dendritic trees having numerous spines, we observed spontaneous hippocalcin-YFP translocation to a set of spines correlated with bursts of postsynaptic currents (Fig. 4, Movie S1; 18.9±1.0 %, 149 translocation events in 65 spines of 8 neurons). Each burst induced hippocalcin-YFP translocation to slightly or completely different set of spines that were active during the respective burst. Hippocalcin-YFP translocation to dendritic shaft locations was also rarely observed. The translocation and bursts of postsynaptic current were completely blocked by APV (40 μM; data not shown). The translocation into spines was tightly spatially restricted to a spine head with no significant changes in hippocalcin-YFP fluorescence in a dendrite at the beginning of the spine neck (16.2 ±

2.1 % in spines versus 0.1 ± 0.7 % near the neck, $p<0.01$; 35 translocation events in 19 spines, 3 neurons; Fig.4Bb) or adjacent dendritic membranes (data not shown). Spines that were separated by a few micrometers on the dendritic tree signalled independently (Fig. 4, Movie S1). Thus, strong activation of single synapses, which induces synaptic NMDAR-dependent Ca^{2+} influx, is sufficient to mediate homosynaptic hippocalcin signalling in conditions when the Mg^{2+} block of the channels is relieved.

Other sources of $[Ca^{2+}]_i$ mobilization do not result in hippocalcin translocation to spines

Further we assessed whether $[Ca^{2+}]_i$ increase induced by VOCC activation alone may result in hippocalcin-YFP translocation to dendritic spines. It has been previously shown that the proximal dendrites of hippocampal pyramidal neurons are different from spines in the expression of different types of VOCC (Yasuda et al., 2006) with substantial contribution to bpAPs of T-, L- and N-types of calcium channels whereas R-type dominate in the latter structures (Bloodgood & Sabatini, 2007). Activation of VOCC channels as a result of bpAPs or membrane depolarization lead to an increase in $[Ca^{2+}]_i$ in dendritic spines (Bloodgood & Sabatini, 2007) and in theory should result in hippocalcin translocation to these structures.

Two different protocols to selectively activate VOCC were used in this series of experiments. First, we applied series of depolarizing stimuli from -70 to 0 mV (10-50 ms at 7 to 20 Hz; 5 neurons) with a total duration of 1 s resembling duration of the bursts. These stimuli did not produce translocation to spines while spontaneous bursts occurring in the very same neurons did (Fig. 4Ca). We have earlier shown that short

bpAP trains (10 APs at 20 Hz) do not induce substantial hippocalcin-YFP translocation in a dendritic tree of hippocampal neurons (Markova et al., 2008). Therefore, we suggested that the applied stimulation could be too mild to induce translocation to spines. Thus, in the next round of experiments neurones revealing spontaneous bursting were challenged with a train of bpAPs (100 APs at 20 Hz) and bpAP-induced hippocalcin-YFP translocation was quantified in spines, in which translocation was induced during the bursts. We found that no translocation was observed in such sites as a consequence of bpAP trains (18.5±2.1% during the bursts and 1.4±0.4% during APs; 28 ROIs, 5 neurones, $p<0.01$; Fig.4Cb). At the same time, these bpAP trains induced robust hippocalcin-YFP translocation to neighbouring sites in a dendritic shaft.

We also tested if simultaneous activation of synaptic and extrasynaptic NMDAR with a temporal profile analogous to one observed during bursting activity generated hippocalcin translocation to spines. To isolate NMDARs from VOCC, neurons were incubated in Mg^{2+}-free media containing CNQX (10 μM) and voltage clamped at -70 mV. We performed imaging of dendritic branches during spontaneous network bursts and during short iontophoretic glutamate applications to dendritic branches under study. Both types of stimulation induced analogous glutamate receptor-dependent postsynaptic currents (Fig. 5) that were completely blocked by APV (data not shown). At the same time hippocalcin-YFP translocation patterns were substantially different for these types of stimuli. Network bursting resulted in hippocalcin-YFP translocation to spines (2 spines in an example shown in Fig. 5Ac) whereas glutamate iontophoresis mainly induced translocation to many neighbouring sites in the dendritic shaft rather than to spines (Fig. 5Ad). Translocation in the dendritic shaft looks obvious taking into account that extrasynaptic NMDAR activation should increase $[Ca^{2+}]_i$ in the dendritic shaft

thereby inducing hippocalcin-YFP translocation in this dendritic compartment. Nevertheless, it is interesting to note that hippocalcin-YFP translocation to spines was practically abolished in spite of synaptic NMDAR activation during glutamate application (20.2±4.7% during the bursts versus -2.4±1.3% during glutamate application, 33 spines, 4 neurons; $p<0.01$; Fig. 5) implying that only particular patterns of synaptic NMDAR activation may lead to hippocalcin signalling into spines.

Thus, the specific spatio-temporal pattern of $[Ca^{2+}]_i$ changes induced by the intrinsic pattern of synaptic NMDAR activation in the dendritic tree of hippocampal neurons is preferentially decoded by hippocalcin translocation to the dendritic spines and no other Ca^{2+} sources can trigger this type of hippocalcin signalling.

Hippocalcin translocation to spines during bursting neuronal activity

As shown above hippocalcin-YFP translocation to dendritic spines occurs when synaptic NMDARs are the only source of Ca^{2+} to trigger this process but it might not be the case during a normal pattern of activity when a neuron is depolarized and/or generates APs simultaneously with NMDAR activation as takes place during the bursts. VOCC Ca^{2+} influx occurring during the burst together with NMDAR-dependent Ca^{2+} influx and the ER Ca^{2+} stores produce another spatio-temporal profile of $[Ca^{2+}]_i$ that in its turn may result in hippocalcin translocation to other membrane targets. Therefore, we tested whether hippocalcin-YFP translocation to spines are physiologically relevant and can occur during native patterns of neuronal activity (Ben Ari, 2001). Neurons were incubated in an extracellular solution with a higher Mg^{2+} concentration (1 mM), that is enough to engage Mg^{2+} block of NMDARs (Monyer et al., 1994), and $GABA_A$ receptor

blockers. Although we observed some changes in bursting activity the bursts could still be reliably induced in a proportion of cultures (most probably due to block of inhibitory synaptic transmission by $GABA_A$ receptor blockers). Time-lapse imaging of transfected neurons showed that robust hippocalcin-YFP translocation to dendritic spines was still present during the bursts (Fig. 6A-D) but not during subthreshold and low-frequency spontaneous activity (data not shown). The translocation to the plasma membrane of dendritic shaft due to simultaneous NMDAR and VOCC activation during the bursts was more frequently observed in this case (red spots in Fig. 6A and C) compared to recordings in a voltage clamp mode when it was relatively rare (Fig. 4A, B). Hippocalcin-YFP fluorescence was simultaneously decreased in certain areas of dendritic tree (green areas in Fig. 6A, C) indicating sites from which hippocalcin-YFP was diffusionally translocated.

The value of translocation was not equal within a given spine head with some pixels having several fold increase in hippocalcin-YFP fluorescence (Fig.6C, D), indicating that hippocalcin-YFP might be inserted in suboptical (in terms of size) areas of plasma membrane reaching an extremely high level of concentration there. An amplitude of translocation transients to spines was comparable with one observed in a voltage clamp mode in Mg^{2+} free extracellular solution (16.9±0.8%, 153 translocation events, 21 spines, 5 neurons; compare Fig.4B and 6B). In line with previous results, the translocation was blocked by APV (75 translocation events in 19 spines during 14 bursts in control and no translocation in the same set of spines during 44 bursts in APV).

Although a block of hippocalcin-YFP translocation to spines by APV suggests involvement of NMDARs in the triggering of this type of synaptic signalling, it is

possible that APV acted by generally changing the excitability of the neuronal network rather than specifically blocking a critical trigger for translocation. Therefore, we tested whether preventing postsynaptic NMDAR activation via Mg^{2+} block by voltage clamping cells at –70 mV during the bursts would decrease the translocation. This manipulation prevented the translocation to spines (-0.7 ± 1.1%, 4 neurones; Fig. 6 Eb, Fb, G). When the same cells were voltage clamped at -40 mV, the spontaneous bursting resulted in hippocalcin-YFP translocation to spines (9.8± 2.1%, $p<0.01$ compared to -70 mV; 17 ROIs; 4 neurons; Fig.6 Ea, Fa, G).

As in a case of Mg^{2+}-free extracellular solution (Fig. 4C) trains of bpAPs (100 stimuli at 20 Hz) led to hippocalcin-YFP translocation in the dendritic shaft rather than to the spines (Fig.6S). A significant difference was found when hippocalcin-YFP translocation in a response to bpAPs was quantified in the morphologically clearly defined spines that revealed hippocalcin-YFP translocation in a response to the bursts (13.3±1.3% during the bursts and -0.6±1.4% during bpAPs; 9 spines, 4 neurons, $p<0.01$; Fig.6S). Thus, activation of VOCCs themselves does not result in hippocalcin translocation to the dendritic spines. These results demonstrate that hippocalcin may signal to different locations of the dendritic tree depending on patterns of neuronal activity, thus decoding these patterns into site-specific activation of its plasma membrane targets.

Different types of VOCC as well as nonlinear interaction between R-type VOCC and NMDARs (Bloodgood & Sabatini, 2007) may contribute to $[Ca^{2+}]_i$ mobilization in dendritic spines initiated by synaptic NMDAR activation. We used L- and R/T type channel antagonists (nimodipine (10 μM) and mibefradil (10 μM), respectively), in the extracellular solution to block VOCC that may substantially contribute to Ca^{2+} influx to the spines during the bursts. We could not block P/Q- and N-types of VOCC since they

secure glutamate release in presynaptic terminals; fortunately, they do not substantially contribute to $[Ca^{2+}]_i$ transients in the spines (Bloodgood & Sabatini, 2007). The VOCC antagonists didn't induce depression of hippocalcin-YFP translocation to spines during the bursts (16.9±0.8% in control and 18.3±1% in the antagonists, 48 spines 5 neurons, p=0.13), implying that synaptic NMDARs are probably the main source of Ca^{2+} influx to spines resulting in hippocalcin translocation.

Discussion

Previous studies have demonstrated that hippocalcin signalling is necessary for spatial and associative memory (Kobayashi et al., 2005) and plays an important role in synaptic plasticity (Palmer et al., 2005) and many other cellular functions (Lindholm et al., 2002; Tzingounis et al., 2007). However, the cellular mechanisms involved in hippocalcin signalling still remain illusive. This is in part because of the lack of temporal resolution of existing experimental approaches (mainly based on immunocytochemical assays) for studies of fast molecular movement and interaction in living cells. Here we used hippocalcin tagged with fluorescent proteins to study hippocalcin translocation induced by fast glutamate receptor activation. By combining electrophysiology with hippocalcin-FP imaging we showed that hippocalcin may differentially decode glutamate receptor activation and that network bursting discharges results in homosynaptic hippocalcin signalling in active dendritic spines.

Dynamic range of hippocalcin concentration changes in the plasma membrane

One of a major consideration for determining the intrinsic dynamics of hippocalcin translocation is that overexpression of recombinant protein should not substantially change its initial pool size and stoichiometry of interaction with target proteins. The endogenous hippocalcin concentration in hippocampal pyramidal cells was estimated to be more than 30 μM (Furuta et al., 1999). This concentration may be the highest among the EF-hand type calcium-binding proteins in these cells, and is comparable to calmodulin concentration (Kakiuchi et al., 1982). Although we did not take any precautions to limit the exogenous protein pool, expression levels comparable to 30 μM are normally not observed in mammalian cells and rarely exceed 10-20 μM (van der

Wal J. et al., 2001). Thus, the exogenous hippocalcin pool was hardly above 50 % of endogenous one. Besides, qualitatively similar results in respect of hippocalcin translocation to spines were obtained in neurons with different (up to 5 times) levels of hippocalcin expression also indicating that overexpression was not crucial for its intrinsic dynamics.

Amplitudes of hippocalcin-YFP translocation transients ranged from several up to 60 % of initial value of hippocalcin-YFP concentration with an averaged value of about 20 %. Thus, a dynamic range of hippocalcin concentration changes in spines looks narrow. However, actual changes of hippocalcin concentration at its site of action - the plasma membrane - might be very substantial allowing hippocalcin to be a fine tuning regulator of its membrane targets. In order to estimate a hippocalcin dynamic range we have to know a real hippocalcin concentration in the plasma membrane at rest and during the bursting. It has been suggested that hippocalcin is mainly cytosolic protein (Kobayashi et al., 1993; Markova et al., 2008). It implies that a tiny part of hippocalcin molecules (if any) is present in the plasma membrane at the resting level of $[Ca^{2+}]_i$. To estimate the amount of hippocalcin-YFP associated with the spine plasma membrane during the burst we took into account the following considerations. First, the spatial distribution of hippocalcin-YFP in the dendritic shaft adjacent to active spines and, consequently cytosolic hippocalcin-YFP concentration, was not changed when neurons were clamped at -70mV during the burst (Fig. 4 Bb). Second, hippocalcin-YFP translocation to spines lasted substantially longer (~5-10s; Fig. 4 Ba) than characteristic time necessary for molecules of hippocalcin size to diffusionally equilibrate via a spine neck (less than 1s) (Majewska et al., 2000; Sharma et al., 2006). Based on the observations above we may suggest that the cytosolic hippocalcin concentration in the spines and adjacent dendritic

shaft is approximately equal at the peak of translocation transients and is the same as before the translocation. Thus, in the first approximation the whole amount of hippocalcin translocated to dendritic spines (up to 60 % of resting level) should be associated with the plasma membrane where just a few percent of total hippocalcin could be present at rest. In other words, hippocalcin concentration in the plasma membrane of spines can be increased dozens of times during robust hippocalcin translocation. Taking into account, that hippocalcin can translocate to diffractionally limited spots within the plasma membrane of spines rather than being randomly associated with the plasma membrane during the translocation (Fig.6 D) the dynamic range of hippocalcin concentration changes in the plasma membrane might be even wider allowing hippocalcin to be a fine-tuning regulator of intracellular signalling events.

Biophysical mechanisms of hippocalcin translocation

One of major findings from this study is that there is no obvious direct relationship between Ca^{2+} influx and hippocalcin translocation. E.g. translocation does not occur in response to both short trains of action potentials (Markova et. al. 2008) and short activation of synaptic NMDARs in spite of the fact that Ca^{2+} influx via VOCCs and NMDARs increases $[Ca^{2+}]_i$ ((Sabatini et al., 2002) and our unpublished results). Translocation to spines is not also observed during vigorous AP stimulation in spite of robust Ca^{2+} influx via VOCCs. Even prolonged synaptic NMDAR activation during glutamate iontophoretic application does not result in hippocalcin translocation to spines. All in all a complex interplay between $[Ca^{2+}]_i$ changes, Ca^{2+}-dependent

hippocalcin transitions between its different states, distribution of local plasma membrane affinities for hippocalcin, hippocalcin interaction with target proteins and particular morphology of dendritic segment determining hippocalcin and Ca^{2+} diffusion results in a specific pattern of hippocalcin translocation. Thus, it is hard to foresee how hippocalcin may locally translocate in response to a certain pattern of neuronal activity and experimental measurements are possibly the only way to figure it out. Nevertheless, some simple considerations might be taken into account to qualitatively describe biophysical mechanisms underlying hippocalcin translocation observed in this study. Here we show that Ca^{2+} influx via synaptic NMDARs is the main mechanism inducing robust hippocalcin translocation to dendritic spines whereas other sources of $[Ca^{2+}]_i$ increase, e.g. VOCC activation by bpAPs, was ineffective in this role. A spatio-temporal profile of $[Ca^{2+}]_i$ in the spines should be considered in order to explain this apparent contradiction. Although each action potential can generate a large $[Ca^{2+}]_i$ transient in the spines, a rapid clearance of Ca^{2+} (about 12 ms (Sabatini et al., 2002)) should prevent a large $[Ca^{2+}]_i$ accumulation in the spines during AP trains used in this study (Fig.7C). Besides, an on-rate of Ca^{2+} binding for many EF-hand type Ca^{2+}-binding proteins are reported to be low (Holmes, 2000) and, therefore, these proteins can be too slow to follow fast $[Ca^{2+}]_i$ transients induced by APs. Since AP-evoked $[Ca^{2+}]_i$ transients in the spines remain at high levels for just several milliseconds they should be ineffective in activating the Ca^{2+}-myristoyl switch of hippocalcin (Fig.7C). Therefore, hippocalcin translocation to the spines was not observed in these conditions.

At the same time a single vesicle of glutamate released in a particular synapse (Fig.7A) resulted in a local $[Ca^{2+}]_i$ increase in spines without substantial $[Ca^{2+}]_i$ increase in the dendritic shaft (Sabatini et al., 2002). A precise compartmentalization of $[Ca^{2+}]_i$ signals

together with its relatively long duration and high amplitude (~100ms and ~10 μM (Sabatini et al., 2002)) could result in hippocalcin translocation. Nevertheless, this local $[Ca^{2+}]_i$ transient did not induce translocation to spines indicating that either the $[Ca^{2+}]_i$ increase was not high or long enough for hippocalcin to bind Ca^{2+} and to induce the Ca^{2+}-myristoyl switch. It is possible that as in the case with calmodulin, the most studied EF-hand type protein, higher $[Ca^{2+}]$ (above 10 μM) is necessary for Ca^{2+} binding to all EF-hand domains (Park et al., 2008) and subsequent fast hippocalcin translocation. Whatever is the reason the translocation following a single synaptic stimulation was negligible, effectively filtering subthreshold synaptic activity. Threshold EPSPs with 1-2 APs riding on the top of these EPSPs (Fig.7A) also did not produce any visible hippocalcin translocation to spines. Thus, the biophysical properties of hippocalcin are ideally suited to skip a single quantum release at the spine level. At the same time bursting activity, that should result in a general increase of $[Ca^{2+}]_i$ in both dendritic shaft and spines, produced strong hippocalcin translocation to spines. Higher affinity for hippocalcin binding to the plasma membrane and larger $[Ca^{2+}]_i$ increase in a spine head compared to a dendritic shaft (Sabatini et al., 2002) might be suggested as potential biophysical mechanisms for the observed spine specificity of hippocalcin insertion in the spine plasma membrane during a strong synaptic input (Fig.7B). Thus far, hippocalcin depletion in the spine head cytosol after its insertion into the spine plasma membrane underlies its diffusion from a parent dendrite via a spine neck (the equilibration time constant of about 100 ms) and its additional insertion in the spine membrane observed as an increase in spine hippocalcin concentration (Fig.7B). Finally, iontophoretic glutamate application that activated the whole set of both synaptic and extrasynaptic glutamate receptors should induce large and prolonged $[Ca^{2+}]_i$ increase in

dendrites and strong hippocalcin translocation to the dendritic plasma membrane. This results in depletion of the cytosolic hippocalcin fraction in a dendritic shaft preventing hippocalcin translocation to the spines (Fig.7 D). Such competition for a limiting amount of hippocalcin among its targets can potentially produce a variety of complex effects including dependence of particular hippocalcin-related activity on the history of hippocalcin translocation to disparate targets.

Possible mechanisms of hippocalcin signalling in neurons

Based on the described biophysical properties hippocalcin may contribute to intracellular signalling in several ways. Its site-specific Ca^{2+}-dependent translocation to the plasma membrane may result in regulation of membrane bound targets spatially segregated in the translocation sites. The higher hippocalcin affinity for membranes of certain composition (O'Callaghan et al., 2005) as well as some protein-protein interaction with possible membrane targets (Haynes et al., 2006; Tzingounis et al., 2007; Tzingounis & Nicoll, 2008) may underlie this type of signalling. A direct interaction of hippocalcin with membranous targets realizing this scenario may be suggested when hippocalcin gates $[Ca^{2+}]_i$-dependent potassium channels responsible for slow (Tzingounis et al., 2007) and medium (Tzingounis & Nicoll, 2008) afterhyperpolarization to regulate neuronal membrane potential and bursting activity.

At the same time, hippocalcin might signal as a ‘shuttle’ delivering specific molecules to their sites of action. At low $[Ca^{2+}]_i$, hippocalcin is likely folded with its N-terminal myristoyl group hidden in a hydrophobic pocket as described for the NCS protein recoverin (Ames et al., 1997). The binding of Ca^{2+} would result in a conformational

switch and protrusion of the N-terminal region out of the pocket. The N-terminus or the exposed hydrophobic region of hippocalcin may interact with cytosolic target proteins in Ca^{2+}-dependent manner (Palmer et al., 2005). Hippocalcin translocation to certain plasma membrane sites would bring the interacting proteins to their sites of action. Ca^{2+} unbinding from hippocalcin would result in hippocalcin dissociation from the interacting protein and its translocation back to the cytosol. If $[Ca^{2+}]_i$ is still high the next round of shuttling would start. Fast and transient hippocalcin translocation to dendritic spines is a biophysical basis for this scenario. It has been also shown that hippocalcin can directly interact in Ca^{2+}-dependent manner with several neuronal cytosolic proteins (Haynes et al., 2006) including ones contributing to NMDAR-dependent AMPAR LTD (Palmer et al., 2005). Although there are Ca^{2+}-independent mechanisms of AMPAR LTD (Dickinson et al., 2009), hippocalcin is specifically required for this Ca^{2+}-dependent form of plasticity. Its N-terminal interaction with a cytosolic protein, β2-adaptin subunit of the AP2 adaptor complex, is necessary for the LTD expression (Palmer et al., 2005). The hippocalcin-AP2 complex interacts with AMPARs leading to AMPAR endocytosis via clathrin-coated vesicles. Moreover, hippocalcin is absent from these vesicles indicating that the interaction between hippocalcin and the AP2-AMPAR complex is transient and may only occur at the plasma membrane supporting the idea about ‘shuttling’ function of hippocalcin at least in this signalling pathway. Fast off-rates of Ca^{2+} binding to EF-hand type proteins are also in line with this suggestion (Bayley et al., 1984).

Finally, after activation of the Ca^{2+}-myristoyl switch, hippocalcin has a high affinity for a phospholipid of the plasma membrane, PIP_2 (O'Callaghan et al., 2005), which is a messenger and precursor of other messenger molecules. Having in mind the high

hippocalcin concentration in the hippocampus (about 30 μM (Furuta et al., 1999)) it could effectively buffer PIP_2 in the plasma membrane locally regulating PIP_2-dependent intracellular signalling.

In conclusion, our data reveal that synaptic AMPAR and NMDAR activation, action potential firing and extrasynaptic glutamate receptor activation produce different spatio-temporal patterns of hippocalcin translocation. Thus, we propose that hippocalcin may differentially decode activation of glutamate receptors converting it to site and time specific modification of its targets. Hippocalcin may also process information in parallel in many sites within a neuron or produce local site-specific signalling at the level of single synapses.

Acknowledgements

This work was supported by Wellcome Trust Grants 069465 (PVB and AVT) and partially supported by INTAS grant (1861). We thank Tetyana Tsugorka for preparing cultures and Dr. Nikolai Kononenko for helpful discussion.

Abbreviations AMPAR, AMPA receptor; AP, action potential; APV, D-2-amino-5-phosphonopentanoic acid; bpAPs , back propagating action potentials; CFP, Cyan Fluorescent Protein; CNQX, 6-cyano-7-nitroquinoxaline-2,3-dione; CPA, cyclopiazonic acid; EPSP, excitatory postsynaptic potential; ER, endoplasmic reticulum; gabazine, 6-Imino-3-(4-methoxyphenyl)-1(6H)-pyridazinebutanoic acid; hippocalcin-YFP, Yellow Fluorescent Protein-tagged hippocalcin; LTD, long-term depression; MCPG, α-methyl-4-carboxyphenylglycine; NCS, neuronal calcium sensor; NMDAR, NMDA receptor; ROI, region of interest; sAHP, slow afterhyperpolarization; VOCC, voltage operated

calcium channel; IP_3, inositol 1,4,5-triphosphate; PIP_2, phosphatidylinositol (4,5)-bisphosphate.

Reference List

Ames,J.B., Ishima,R., Tanaka,T., Gordon,J.I., Stryer,L. & Ikura,M. (1997) Molecular mechanics of calcium-myristoyl switches. *Nature*, **389**, 198-202.

Bardo,S., Cavazzini,M.G. & Emptage,N. (2006) The role of the endoplasmic reticulum Ca2+ store in the plasticity of central neurons. *Trends Pharmacol Sci.*, **27**, 78-84.

Bayley,P., Ahlstrom,P., Martin,S.R. & Forsen,S. (1984) The kinetics of calcium binding to calmodulin: Quin 2 and ANS stopped-flow fluorescence studies. *Biochem.Biophys.Res.Commun.*, **120**, 185-191.

Ben Ari,Y. (2001) Developing networks play a similar melody. *Trends Neurosci*, **24**, 353-360.

Bezprozvanny,I. (2005) The inositol 1,4,5-trisphosphate receptors. *Cell Calcium*, **38**, 261-272.

Bloodgood,B.L. & Sabatini,B.L. (2007) Nonlinear regulation of unitary synaptic signals by CaV(2.3) voltage-sensitive calcium channels located in dendritic spines. *Neuron*, **53**, 249-260.

Braunewell,K.H. (2005) The darker side of Ca2+ signaling by neuronal Ca2+-sensor proteins: from Alzheimer's disease to cancer. *Trends Pharmacol.Sci.*, **26**, 345-351.

Burgoyne,R.D., O'Callaghan,D.W., Hasdemir,B., Haynes,L.P. & Tepikin,A.V. (2004) Neuronal Ca2+-sensor proteins: multitalented regulators of neuronal function. *Trends Neurosci.*, **27** , 203-209.

Dickinson,B., Jo,J., Seok,H., Son,G., Whitcomb,D., Davies,C., Sheng,M., Collingridge,G. & Cho,K. (2009) A novel mechanism of hippocampal LTD involving muscarinic receptor-triggered interactions between AMPARs, GRIP and liprin-alpha. *Molecular Brain*, **2**, 18.

Furuta,Y., Kobayashi,M., Masaki,T. & Takamatsu,K. (1999) Age-related changes in expression of hippocalcin and NVP2 in rat brain. *Neurochem.Res.*, **24**, 651-658.

Haynes,L.P., Fitzgerald,D.J., Wareing,B., O'Callaghan,D.W., Morgan,A. & Burgoyne,R.D. (2006) Analysis of the interacting partners of the neuronal calcium-binding proteins L-CaBP1, hippocalcin, NCS-1 and neurocalcin delta. *Proteomics.*, **6**, 1822-1832.

Holmes,W.R. (2000) Models of calmodulin trapping and CaM kinase II activation in a dendritic spine. *J Comput.Neurosci*, **8**, 65-85.

Jinno,S., Jeromin,A. & Kosaka,T. (2004) Expression and possible role of neuronal calcium sensor-1 in the cerebellum. *Cerebellum.*, **3**, 83-88.

Jo,J., Heon,S., Kim,M.J., Son,G.H., Park,Y., Henley,J.M., Weiss,J.L., Sheng,M., Collingridge,G.L. & Cho,K. (2008) Metabotropic glutamate receptor-mediated LTD involves two interacting Ca(2+) sensors, NCS-1 and PICK1. *Neuron*, **60**, 1095-1111.

Kakiuchi,S., Yasuda,S., Yamazaki,R., Teshima,Y., Kanda,K., Kakiuchi,R. & Sobue,K. (1982) Quantitative determinations of calmodulin in the supernatant and particulate fractions of mammalian tissues. *J Biochem.*, **92**, 1041-1048.

Kobayashi,M., Masaki,T., Hori,K., Masuo,Y., Miyamoto,M., Tsubokawa,H., Noguchi,H., Nomura,M. & Takamatsu,K. (2005) Hippocalcin-deficient mice display a defect in cAMP response element-binding protein activation associated with impaired spatial and associative memory. *Neuroscience*, **133**, 471-484.

Kobayashi,M., Takamatsu,K., Saitoh,S. & Noguchi,T. (1993) Myristoylation of hippocalcin is linked to its calcium-dependent membrane association properties. *J Biol.Chem.*, **268**, 18898-18904.

Korhonen,L., Hansson,I., Kukkonen,J.P., Brannvall,K., Kobayashi,M., Takamatsu,K. & Lindholm,D. (2005) Hippocalcin protects against caspase-12-induced and age-dependent neuronal degeneration. *Mol.Cell Neurosci.*, **28**, 85-95.

Lindholm,D., Mercer,E.A., Yu,L.Y., Chen,Y., Kukkonen,J., Korhonen,L. & Arumae,U. (2002) Neuronal apoptosis inhibitory protein: Structural requirements for hippocalcin binding and effects on survival of NGF-dependent sympathetic neurons. *Biochim.Biophys.Acta*, **1600**, 138-147.

Lu,W., Man,H., Ju,W., Trimble,W.S., MacDonald,J.F. & Wang,Y.T. (2001) Activation of synaptic NMDA receptors induces membrane insertion of new AMPA receptors and LTP in cultured hippocampal neurons. *Neuron* , **29**, 243-254.

Majewska,A., Tashiro,A. & Yuste,R. (2000) Regulation of spine calcium dynamics by rapid spine motility. *J Neurosci*, **20**, 8262-8268.

Mangan,P.S. & Kapur,J. (2004) Factors underlying bursting behavior in a network of cultured hippocampal neurons exposed to zero magnesium. *J Neurophysiol*, **91**, 946-957.

Markova,O., Fitzgerald,D., Stepanyuk,A., Dovgan,A., Cherkas,V., Tepikin,A., Burgoyne,R.D. & Belan,P. (2008) Hippocalcin signaling via site-specific translocation in hippocampal neurons. *Neurosci.Lett.*, **442**, 152-157.

McFerran,B.W., Graham,M.E. & Burgoyne,R.D. (1998) Neuronal Ca2+ sensor 1, the mammalian homologue of frequenin, is expressed in chromaffin and PC12 cells and regulates neurosecretion from dense-core granules. *J Biol.Chem.*, **273**, 22768-22772.

Melnick,I.V., Chvanov,M.A. & Belan,P.V. (1999) Rat hippocampal neurons maintain their own GABAergic synaptic transmission in culture. *Neurosci Lett*, **262**, 151-154.

Micheva,K.D., Holz,R.W. & Smith,S.J. (2001) Regulation of presynaptic phosphatidylinositol 4,5-biphosphate by neuronal activity. *J Cell Biol.*, **154**, 355-368.

Monyer,H., Burnashev,N., Laurie,D.J., Sakmann,B. & Seeburg,P.H. (1994) Developmental and regional expression in the rat brain and functional properties of four NMDA receptors. *Neuron,* **12**, 529-540.

O'Callaghan,D.W., Haynes,L.P. & Burgoyne,R.D. (2005) High-affinity interaction of the N-terminal myristoylation motif of the neuronal calcium sensor protein hippocalcin with phosphatidylinositol 4,5-bisphosphate. *Biochem.J,* **391**, 231-238.

O'Callaghan,D.W., Ivings,L., Weiss,J.L., Ashby,M.C., Tepikin,A.V. & Burgoyne,R.D. (2002) Differential use of myristoyl groups on neuronal calcium sensor proteins as a determinant of spatio-temporal aspects of Ca2+ signal transduction. *J Biol.Chem.,* **277**, 14227-14237.

O'Callaghan,D.W., Tepikin,A.V. & Burgoyne,R.D. (2003) Dynamics and calcium sensitivity of the Ca2+/myristoyl switch protein hippocalcin in living cells. *J Cell Biol.,* **163**, 715-721.

Palmer,C.L., Lim,W., Hastie,P.G., Toward,M., Korolchuk,V.I., Burbidge,S.A., Banting,G., Collingridge,G.L., Isaac,J.T. & Henley,J.M. (2005) Hippocalcin Functions as a Calcium Sensor in Hippocampal LTD. *Neuron,* **47**, 487-494.

Park,H.Y., Kim,S.A., Korlach,J., Rhoades,E., Kwok,L.W., Zipfel,W.R., Waxham,M.N., Webb,W.W. & Pollack,L. (2008) Conformational changes of calmodulin upon Ca2+ binding studied with a microfluidic mixer. *PNAS,* **105**, 542-547.

Sabatini,B.L., Oertner,T.G. & Svoboda,K. (2002) The life cycle of Ca(2+) ions in dendritic spines. *Neuron,* **33**, 439-452.

Sharma,K., Fong,D.K. & Craig,A.M. (2006) Postsynaptic protein mobility in dendritic spines: long-term regulation by synaptic NMDA receptor activation. *Mol.Cell Neurosci,* **31**, 702-712.

Teruel,M.N. & Meyer,T. (2000) Translocation and reversible localization of signaling proteins: a dynamic future for signal transduction. *Cell,* **103**, 181-184.

Tzingounis,A.V., Kobayashi,M., Takamatsu,K. & Nicoll,R.A. (2007) Hippocalcin gates the calcium activation of the slow afterhyperpolarization in hippocampal pyramidal cells. *Neuron,* **53**, 487-493.

Tzingounis,A.V. & Nicoll,R.A. (2008) Contribution of KCNQ2 and KCNQ3 to the medium and slow afterhyperpolarization currents. *Proc.Natl.Acad.Sci.U.S.A,* **105**, 19974-19979.

van der Wal J., Habets,R., Varnai,P., Balla,T. & Jalink,K. (2001) Monitoring agonist-induced phospholipase C activation in live cells by fluorescence resonance energy transfer. *J Biol.Chem.,* **276**, 15337-15344.

Walther,H., Lambert,J.D., Jones,R.S., Heinemann,U. & Hamon,B. (1986) Epileptiform activity in combined slices of the hippocampus, subiculum and entorhinal cortex during perfusion with low magnesium medium. *Neurosci Lett.,* **69**, 156-161.

Yasuda,R., Harvey,C.D., Zhong,H., Sobczyk,A., van Aelst,L. & Svoboda,K. (2006) Supersensitive Ras activation in dendrites and spines revealed by two-photon fluorescence lifetime imaging. *Nat.Neurosci.*, **9**, 283-291.

Zheng,Q., Bobich,J.A., Vidugiriene,J., McFadden,S.C., Thomas,F., Roder,J. & Jeromin,A. (2005) Neuronal calcium sensor-1 facilitates neuronal exocytosis through phosphatidylinositol 4-kinase. *J Neurochem.*, **92**, 442-451.

Figure legends

Figure 1. Local iontophoretic glutamate application induced hippocalcin-YFP translocation in cultured hippocampal neurons. **A.** A set of images demonstrating glutamate-induced changes in hippocalcin-YFP fluorescence in an apical dendrite of iontophoretically stimulated neuron. The fluorescent image (**a**) was taken using theYFP filter set. The position of the iontophoretic pipette is indicated by dashed lines. **Ab**. A higher magnification image of a dendritic branch shown in a boxed area in **Aa**. Differential pseudocolor images were taken at 2.5 sec after the onset of short iontophoretic glutamate stimulation in control (**c**), in APV and CNQX (**d**), and after blocker washout (**e**). In this and other figures a green colour represents a decrease and red represents an increase in hippocalcin-YFP fluorescence. Colour arrows in **c** indicate sites where regions of interest (ROIs) were placed. Time courses of fluorescence changes in these ROIs in control, APV and CNQX, and after blocker washout are shown in **B**. Colours of traces match arrow colours in **Ab**. Onsets of iontophoretic glutamate applications are shown by black arrows. **C**. Representative (taken from 7 ROIs in the experiment shown in **A**)(**a**) and pooled (46 ROIs, 6 neurons) (**b**) graphs showing a complete suppression of hippocalcin-YFP translocation by ionotropic glutamate receptor blockers.

Figure 2. AMPAR activation resulted in hippocalcin-YFP translocation due to Ca^{2+} influx via voltage-gated calcium channels. Experiments were conducted in a constant presence of APV (40 μM) in order to block NMDARs. **A.** A set of images demonstrating AMPAR-dependent hippocalcin-YFP translocation in a neuron stimulated by iontophoretically applied glutamate. A fluorescent image (**a**) was taken using YFP filter set. The position of the iontophoretic pipette is indicated by dashed lines. **Ab**. A higher magnification image of a dendritic branch shown in a boxed area in **Aa**. Differential pseudocolor images were taken at 3 sec after an onset of iontophoretic glutamate application (1.0s, 100nA) in control (**c**) and CNQX-containing (**d**) solutions, and after CNQX washout (**e**). An outline of dendritic tree is shown in each pseudocolor image for better visualization of translocation sites. Colour arrows in **Ab** indicate sites where ROIs were placed. Time courses of fluorescence changes in these ROIs in control, CNQX (10 μM), and after the blocker washout are shown in **B**. Colours of traces match arrow colours in **Ab**. Onsets of iontophoretic glutamate applications are shown by black arrows. **C**. Pooled results (3 neurons; 65 ROIs) demonstrating a complete suppression of hippocalcin-YFP translocation by CNQX. **D.** Hippocalcin-YFP translocation induced by different stimulation protocols: voltage (**a)** (-70 mV, (VC)) and current **(b)** clamp (CC) combined with iontophoretic glutamate application (1.0s, 100nA); intracellular stimulation with 100 bpAPs at 20Hz (APs) with no glutamate application conducted (**c)**. A red trace represents a ROI with an increase of hippocalcin-YFP fluorescence whereas a green one represents a ROI with a fluorescence decrease; black traces represent changes in membrane currents (**a**) and potential (**b, c**), respectively. **E**. Pooled (5 neurons) results showing a significant suppression of

hippocalcin-YFP translocations in VC mode and comparable translocations in CC and bpAPs.

Figure 3. Hippocalcin-YFP translocated due to direct Ca^{2+} influx via NMDARs.

A. Images demonstrating NMDAR-dependent hippocalcin-YFP translocation in a neuron stimulated by iontophoretically applied glutamate in Mg^{2+}-free solution in a presence of CNQX (10μM), gabazine (5μM) and glycine (10μM). A fluorescent image (**a**) was taken using the YFP filter set. The position of the iontophoretic pipette is indicated by dashed lines. **Ab**. A higher magnification image of a dendritic branch shown in a boxed area in **Aa**. Differential pseudocolor images were taken at 2.5 sec after an onset of iontophoretic glutamate application (0.5s, 100nA) in control (**c**) and APV-containing (**d**) solutions, and after APV washout (**e**). Colour arrows in **b** indicate sites where ROIs were placed. Time courses of fluorescence changes in these ROIs in control, APV (40 μM), and after the blocker washout are shown in **B**. Colours of traces match arrow colours in **Ab**. Onsets of iontophoretic glutamate applications are shown by black arrows in **B**. The currents (black traces) were recorded in a voltage clamp mode at -60mV to abolish Ca^{2+} influx via VOCC and leave NMDARs as the only source of Ca^{2+} influx. **C.** Representative (taken from 5 ROIs in the experiment shown in **A**) (**a**) and pooled (**b**) (5 neurons, 34 ROIs) graphs showing a strong suppression of hippocalcin-YFP translocation by APV. **D**. Hippocalcin-YFP translocation due to local activation of NMDARs and site-specific association of hippocalcin-YFP with the plasma membrane. A diffusional wave of glutamate released from a pipette (shown by dashed lines in **a**) during an iontophoretic pulse (200 ms, 100 nA; an onset of application is indicated by a black arrow in **b**) initially induced hippocalcin-YFP translocation in a dendritic branch in a site proximal to the pipette (red arrow), after that in more distal site indicated by a green arrow and finally in the most distal sites (blue and cyan arrows). Colour coding of traces in (**b**) matches the colours of arrows in (**a**).

The distance from the pipette tip to the most distal ROI is about 50μm and glutamate wave passed this distance for about 3s that is in an agreement with an estimated rate of glutamate diffusion in the extracellular solution. There was no translocation in more distal dendritic sites indicating that glutamate did not reach NMDARs in these sites.

Figure 4. Strong activation of synaptic NMDARs induced hippocalcin-YFP translocation to dendritic spines.

A. An overlay of morphological (white) and hippocalcin-YFP translocation (red) images of neuron during a spontaneous burst of synaptic NMDAR-dependent currents at the time indicated as ***d*** in **Ba**. All synapses that were active during the burst appear in red. **b-e** demonstrate overlays of morphological (white) and translocation images taken at the moments indicated by respective letters in *Italic* in **Ba**. Colour arrows indicate spines for which time courses of hippocalcin-YFP translocation are demonstrated in **Ba**. NMDAR-dependent currents were simultaneously recorded in a whole-cell voltage clamp (holding potential -70mV) and shown in **Ba** (a black trace). **Bb**. Values of hippocalcin-YFP translocation to spines compared to ones in dendritic tree at 1 μm from the respective spines. **C**. Hippocalcin-YFP translocation to spines in response to membrane depolarization and to NMDAR-dependent synaptic current. An example of hippocalcin-YFP fluorescence changes and simultaneously recorded transmembrane current is shown in **Ca**. In this example, a spontaneous NMDAR-dependent postsynaptic current developed due to a network burst right after the train of depolarizing pulses (7 pulses from -70 to 0 mV; 50 ms at 10Hz). It is clear that the current via synaptic NMDARs rather than the train induced hippocalcin-YFP translocation. In all neurons tested with this particular protocol (n=5; at least 2 trains for each neuron) no translocation was observed as a result of the trains. **Cb**. Pooled results showing that a vigorous bpAP train (100 APs at 20 Hz) did not lead to hippocalcin-YFP translocation to sites where bursting-induced translocation was observed. At the same time, the trains did induce hippocalcin-YFP translocation to neighbouring sites in the dendritic shaft. ROIs were only placed over sites where bursting-induced hippocalcin-

YFP translocation was observed. Experiments were conducted in CNQX, gabazine, glycine, and without Mg^{2+}.

Figure 5. Activation of synaptic and total pools of NMDARs resulted in differential hippocalcin-YFP signalling in spines.

A. Spatial patterns of hippocalcin-YFP translocation induced by activation of synaptic and total (synaptic and extrasynaptic) pools of NMDARs. The synaptic pool was activated during spontaneous network bursts whereas the total pool was stimulated by iontophoretic glutamate application to a neuronal dendritic branch. A fluorescent image (**a**) was taken using YFP filter set. The position of the iontophoretic pipette is indicated by dashed lines. **Ab**. A higher magnification image of a dendritic branch shown in a boxed area in **Aa**. **Ac** and **Ad** demonstrate translocation images taken at the moments indicated by respective letters in *Italic* in **B**. These differential pseudocolor images were taken after an onset of network burst (**c**) and of iontophoretic glutamate application (0.5s, 100nA) (**d**). An outline of dendritic tree is shown in each pseudocolor image for better visualization of translocation sites. Colour arrows in **Ab** indicate sites where ROIs were placed. Time courses of fluorescence changes in these ROIs are shown in **B**. Colours of traces match arrow colours in **Ab**. An onset of iontophoretic glutamate application is shown by a black arrow in **B**. The postsynaptic current (black trace) was recorded in a voltage clamp mode at -70mV to abolish Ca^{2+} influx via VOCC and leave NMDARs as the only source of Ca^{2+} influx. **C**. Pooled results (33 spines in 4 neurons) demonstrating that hippocalcin-YFP translocates to dendritic spines during synaptic rather than both synaptic and extrasynaptic NMDAR activation.

Experiments were conducted in CNQX, gabazine, glycine and without Mg^{2+} in an extracellular solution in order to isolate NMDAR-dependent currents and to relieve them from Mg^{2+} block.

Figure 6. Intrinsic bursts of network activity induced hippocalcin-YFP translocation to dendritic spines.

A. An overlay of hippocalcin-YFP fluorescent image and pseudocolor image demonstrating in red hippocalcin-YFP translocation sites at the moment indicated by a black arrow in **B**. Colour arrows in **A** indicate spines in which changes of fluorescence during bursting activity are demonstrated in **B** with the same colour coding. Changes in the neuronal membrane potential were simultaneously recorded and shown in **B** as a black trace. The translocation occurred in a normal extracellular solution (no glutamate receptor blockers and 1 mM of Mg^{2+}) with 1 μM of gabazine to decrease inhibition in order to induce bursting network activity. Not all spines showed an increase in hippocalcin-YFP fluorescence in response to a particular spontaneous network burst (compare red and green traces in **B**). A part of dendritic tree indicated as a white square in **A** is shown in **C** with higher magnification. **D**. A time course of hippocalcin-YFP fluorescent changes along a yellow line in **C** (Distance '0' represents a yellow line end opposite to a dendritic head). **E, F**. Hippocalcin-YFP translocation to spines was due to direct Ca^{2+} influx via NMDARs rather than due to other mechanisms related to the bursting network activity. Hippocalcin-YFP translocation induced by spontaneous bursting activity was recorded in a neuron voltage clamped at -40mV (**Ea, Fa**) and -70mV (**Eb, Fb**) in order to relieve and engage Mg^{2+} block of NMDARs, respectively. **E**. An overlay of morphological (white) and hippocalcin-YFP translocation image of neuron taken at the moment indicated by black arrows in **F**. Colour arrows in **Ea** indicate spines in which fluorescent changes during bursting activity are demonstrated in **F** with the same colour coding. Changes in the neuronal membrane current were

simultaneously recorded and shown in **F** as black traces. **G**. Comparison of hippocalcin-YFP translocation amplitudes in spines at -40 and-70 mV (4 neurons, 17 ROIs).

Figure 7. Hippocalcin translocation differentially decodes distinct patterns of $[Ca^{2+}]_i$ changes induced by glutamate receptor activation.

Schematic of $[Ca^{2+}]_i$ changes and hippocalcin translocation in a part of dendritic tree. The respective neuronal electrical activity is shown in the right part of the figure. Deeper hues of red show higher $[Ca^{2+}]_i$ levels. Circles with a dash inside and outside denote free and Ca^{2+}-bound forms of hippocalcin, respectively. Thicker lines show high affinity plasma membrane sites.

A. Single subthreshold and threshold EPSPs induce $[Ca^{2+}]_i$ transient limited to a specific spine with no visible hippocalcin translocation. **B.** Several glutamate vesicles successively released in the same active synapse during the burst induce a larger and longer $[Ca^{2+}]_i$ transient leading to robust hippocalcin translocation only to such spines. **C.** A train of bpAPs can not form spatio-temporal pattern of $[Ca^{2+}]_i$ necessary for hippocalcin translocation to the spines rather resulting in lower and slower (compared to burst-induced spine translocation) hippocalcin accumulation in high affinity (‘sticky’) plasma membrane sites of the dendritic tree. **D.** Glutamate spillover induces local activation of synaptic and extrasynaptic NMDARs. The respective local Ca^{2+} influx results in hippocalcin translocation to ‘sticky’ dendritic sites in this local dendritic area. A decreased cytosolic hippocalcin concentration in the dendritic tree prevents hippocalcin translocation to the spines in spite of synaptic NMDAR activation.

Supporting Information

1. Movie S1. Activation of synaptic NMDARs induces hippocalcin-YFP translocation to dendritic spines

3. Figure 6S. VOCC activation did not result in hippocalcin-YFP translocation to dendritic spines.

Spatial patterns of hippocalcin-YFP translocation induced by a spontaneous burst of presynaptic activity (**Aa, Ba**) and by a long train of bpAPs (20Hz, 5 s) (**Ab, Bb**). Spines to which hippocalcin-YFP was translocated are shown by red arrows in **Aa** while a site where translocation was observed in response to bpAPs is shown by a green arrow in **Ab**. Colour coding of traces in **Ba** and **Bb** matches the colours of the arrows. **C**. Pooled results (9 spines, 4 neurons) demonstrating absence of hippocalcin-YFP translocation to dendritic spines during bpAPs. Only clearly morphologically defined spines revealing hippocalcin-YFP translocation in a response to spontaneous bursts were included in statistics.

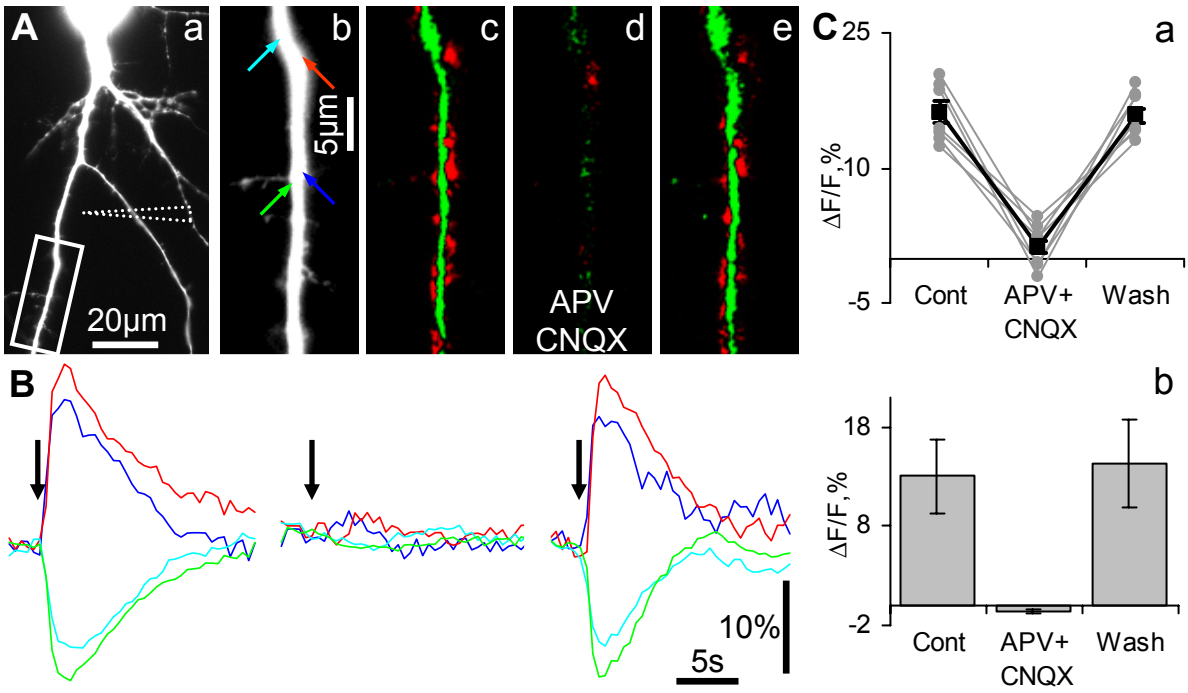
A
a
20μm
b
5μm
c
d
APV
CNQX
e
B
10%
5s
C
a
25
10
-5
ΔF/F,%
Cont
APV+
CNQX
Wash
b
18
8
-2
ΔF/F,%
Cont
APV+
CNQX
Wash

Figure 1

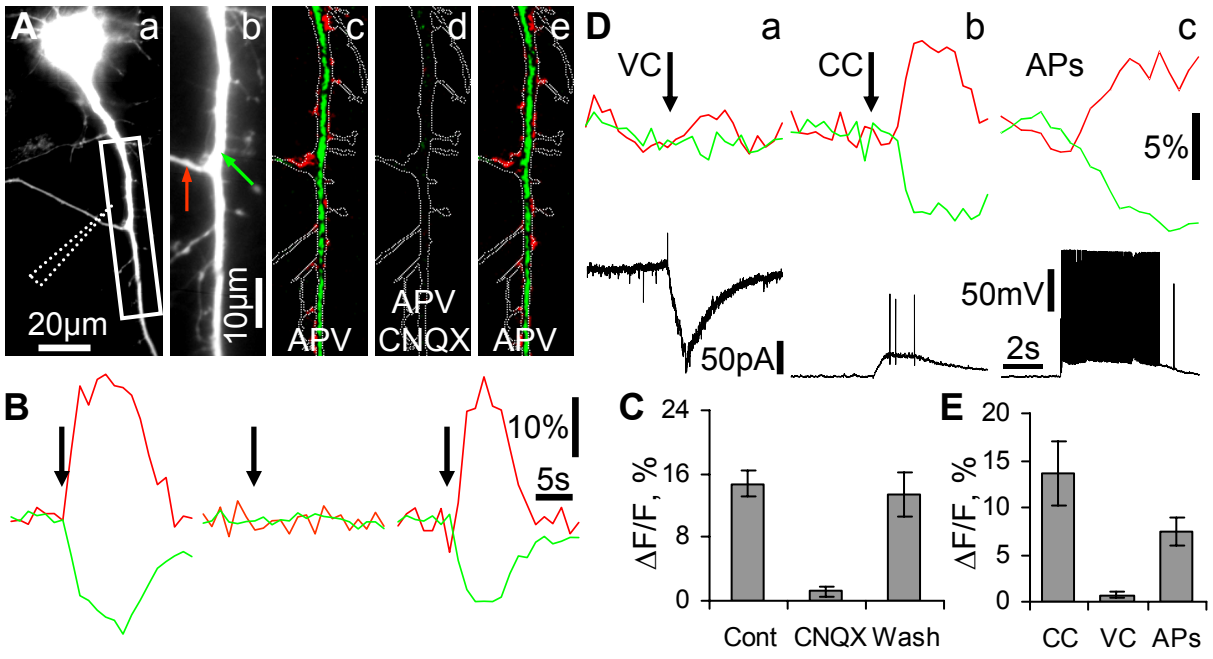
A
a
b
c
d
e
20μm
10μm
APV
APV
CNQX
APV
B
10%
5s
D
a
b
c
VC
CC
APs
5%
50pA
50mV
2s
C
24
16
8
0
ΔF/F, %
Cont
CNQX
Wash
E
20
15
10
5
0
ΔF/F, %
CC
VC
APs

Figure 2

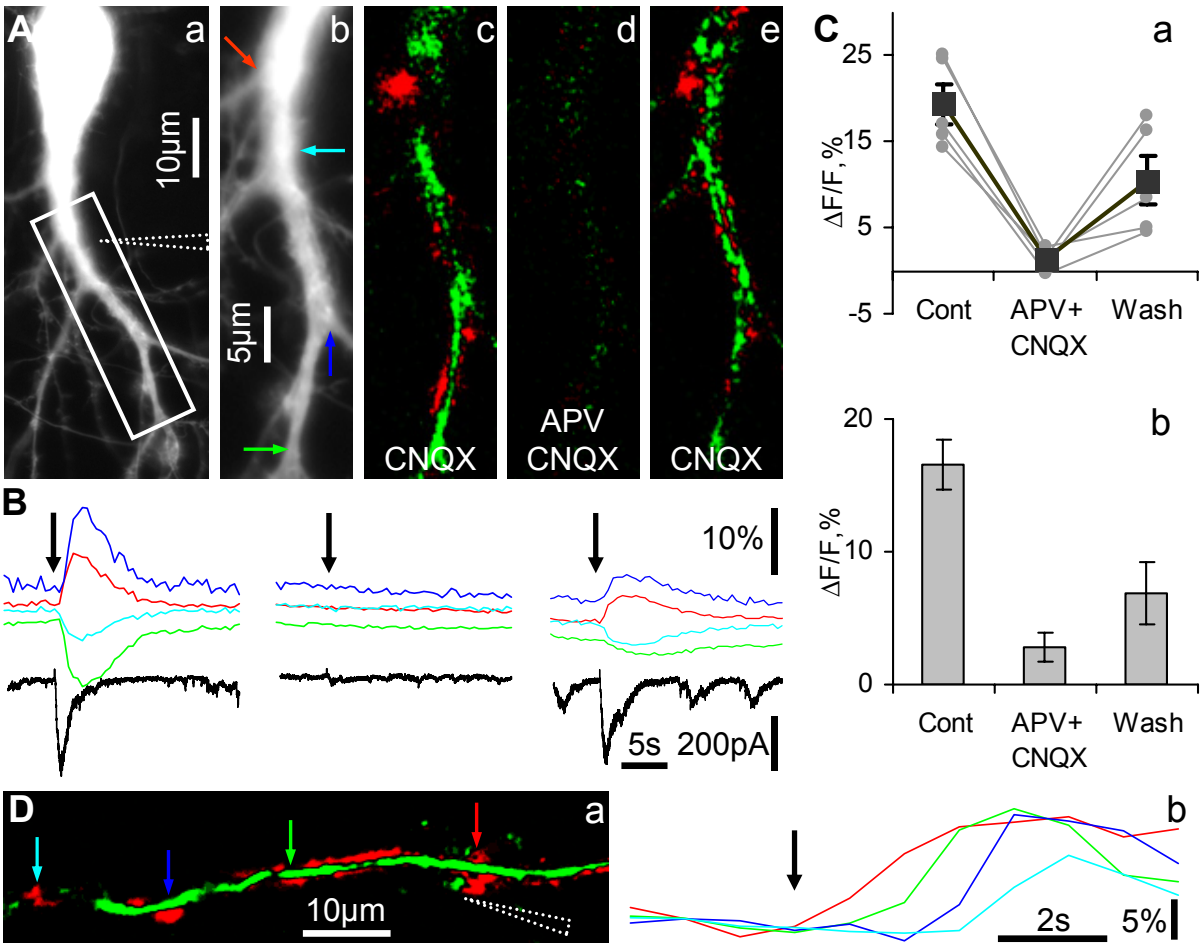
A
a
10μm
b
5μm
c
CNQX
d
APV
CNQX
e
CNQX
B
10%
5s 200pA
C
a
25
15
5
-5
ΔF/F, %
Cont
APV+
CNQX
Wash
b
20
10
0
ΔF/F, %
Cont
APV+
CNQX
Wash
D
a
10μm
b
2s
5%

Figure 3

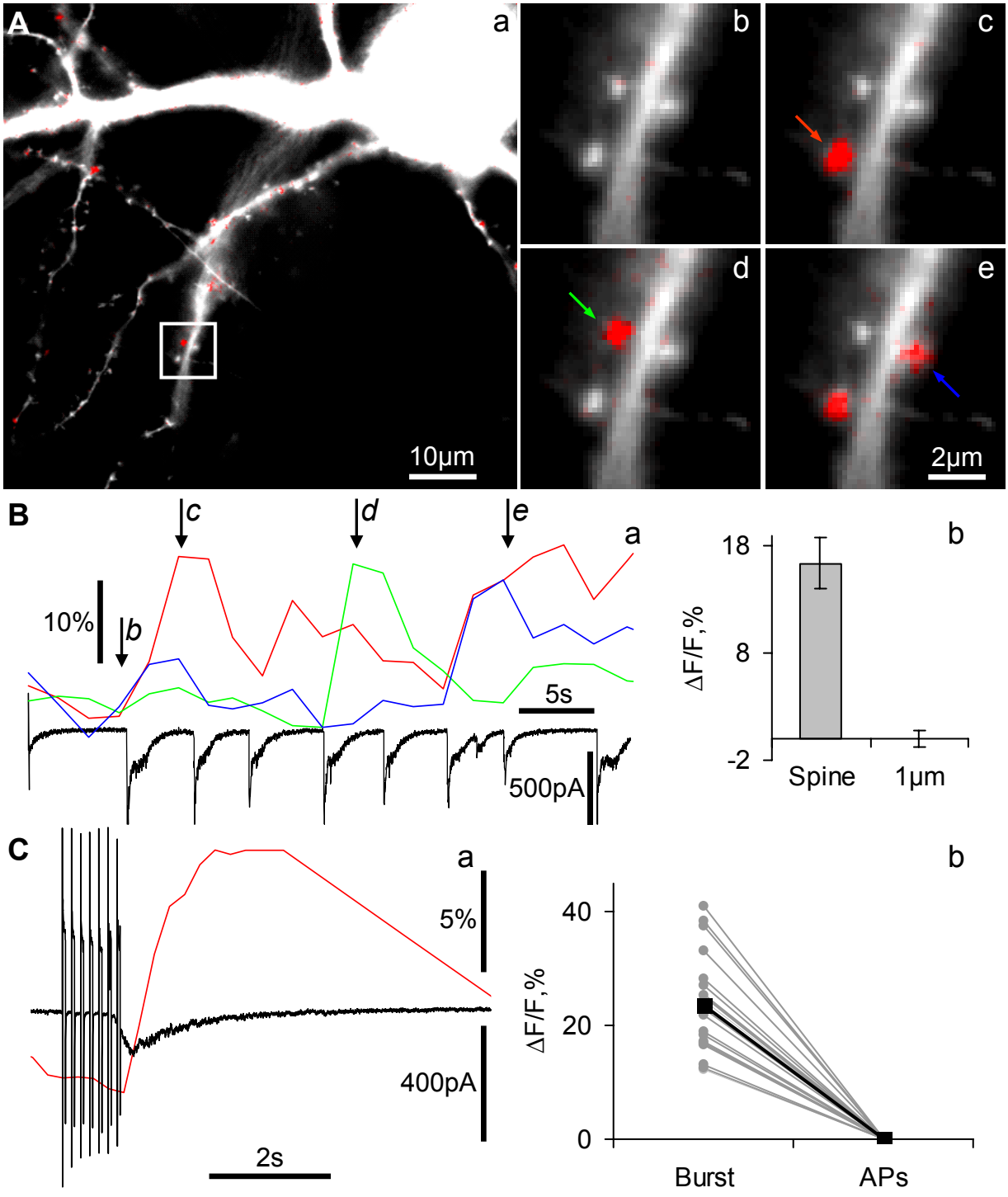
A
a
b
c
d
e
10µm
2µm
B
c
d
e
a
10%
b
5s
500pA
b
18
8
-2
ΔF/F,%
Spine
1µm
C
a
5%
400pA
2s
b
40
20
0
ΔF/F,%
Burst
APs

Figure 4

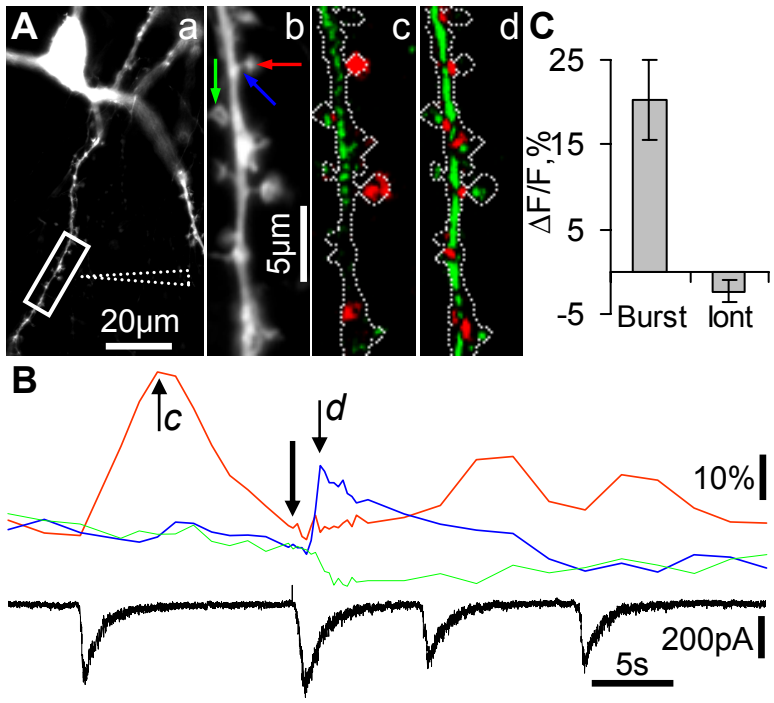

Figure 5

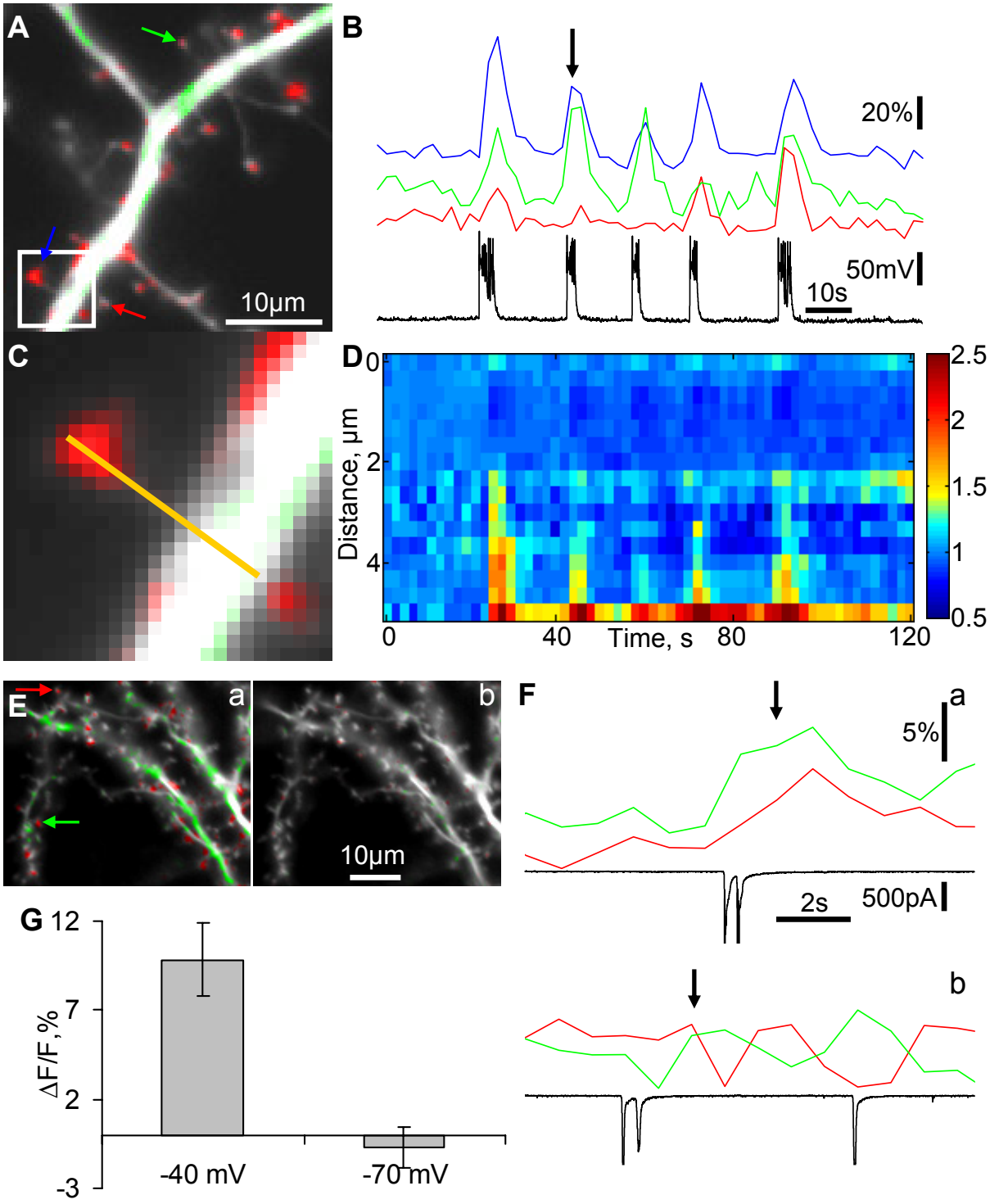
A
10μm
B
20%
50mV
10s
C
D
Distance, μm
0
2
4
0
40
Time, s
80
120
2.5
2
1.5
1
0.5
E
a
b
10μm
F
a
5%
2s
500pA
b
G
12
7
2
-3
ΔF/F,%
-40 mV
-70 mV

Figure 6

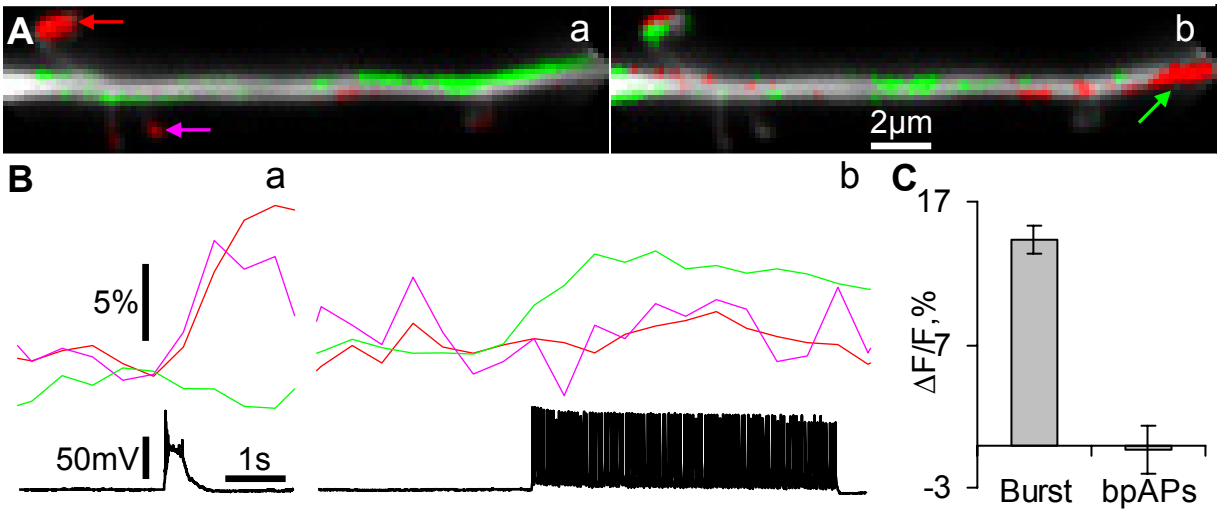

Figure 6s

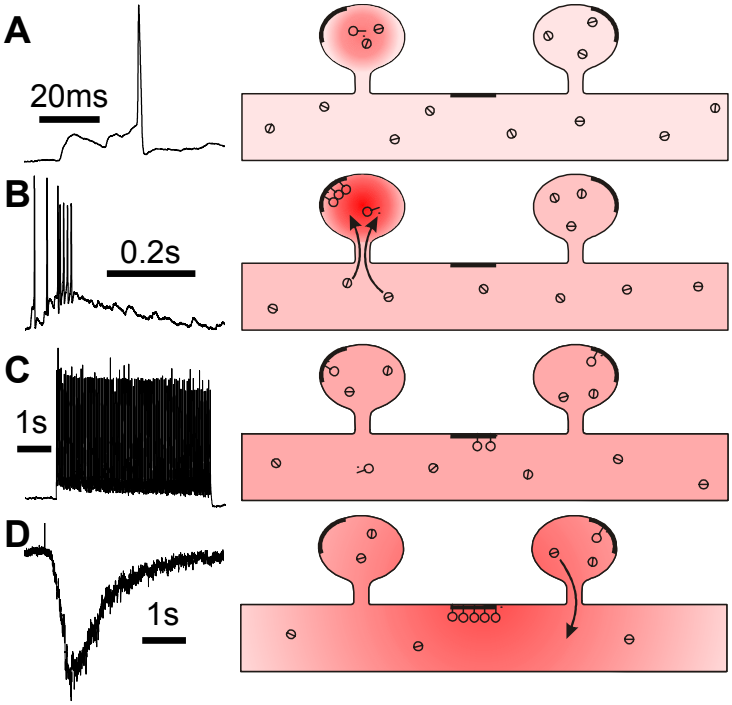

Figure 7